Dalton Transactions

Accepted Manuscript

ROYAL SOCIETY OF CHEMISTRY

www.rsc.org/dalton

Novel chromium(III)-based luminescent metal-organic framework, $[(CH_3)_2NH_2][Na_{0.5}Cr_{0.5}(HCOO)_3]$, was synthesized. This compound crystallizes in a perovskite architecture, space group $R\bar{3}$.

Synthesis and Characterization of $[(CH_3)_2NH_2][Na_{0.5}Cr_{0.5}(HCOO)_3]$: Rare Example of Luminescent Metal-Organic Framework Based on Cr(III) Ions

Mirosław Mączka,*[,a] Bartosz Bondzior,[a] Przemysław Dereń, [a] Adam Sieradzki,[b] Justyna Trzmiel,[b] Adam Pietraszko,[a] and J. Hanuza[a]

[a]*Institute of Low Temperature and Structure Research, Polish Academy of Sciences, Box 1410, 50-950 Wrocław 2, Poland*

[b]*Faculty of Fundamental Problems of Technology, Wrocław University of Technology, Wybrzeże Wyspiańskiego 27, 50-370, Wrocław, Poland*

ABSTRACT

Novel formate $[(CH_3)_2NH_2][Na_{0.5}Cr_{0.5}(HCOO)_3]$ (DMNaCr) was prepared by a solvothermal method. This compound crystallizes in the perovskite-type metal formate framework (space group $R\bar{3}$) with disordered dimethylammonium (DMA^{+}) cations. X-ray diffraction, DSC, Raman and IR studies show that contrary to isostructural iron analogue, $[(CH_3)_2NH_2][Na_{0.5}Fe_{0.5}(HCOO)_3]$ (DMNaFe), DMNaCr does not exhibit any structural phase transition at low temperatures. This behavior has been attributed to smaller flexibility of the perovskite-like framework in DMNaCr when compared with DMNaFe. Dielectric permittivity

data reveal pronounced dielectric relaxation that is attributed to dynamical rotation of DMA^+ ions. Electron absorption and photoluminescence studies show that this material exhibits efficient emission at low temperatures. Detailed analysis of the optical properties shows that chromium ions are located at site of intermediate crystal field strength with Dq/B = 2.29.

Introduction

Metal-organic frameworks (MOFs) are fascinating compounds that received a lot of attention in recent years since combinations of different metal ions and organic ligands enable design of materials with various functionalities such as ferroelectricity, catalytic properties and magnetism.[1,2] They are also attractive luminescent materials, sensors and materials for gas sorption.[2-4] Metal formate frameworks with general formula [cat][$M(HCOO)_3$], where M=Mg, Zn, Mn, Ni, Co, Fe, and cat = ammonium and alkylammonium cations, constitute a subset of MOFs that is known to exhibit interesting magnetic, ferroelectric and gas sorption properties.[5-9] Interest in these compounds increased enormously in the last few years since some of them exhibit multiferroic properties.[10] Luminescent properties of [cat][$M(HCOO)_3$] compounds with divalent metal cations have not been studied yet. It is worth noting however that remarkable emission intensity was observed for rare-earth formate, [(FMD)][$Tb(HCOO)_4$], where FMD denotes formamidinium cation.[11]

Very recently, we have discovered that metal formate, DMNaFe, adopting the perovskite architecture (space group $R\bar{3}$) may be synthesized by mild hydrothermal method.[12] Presence of the trivalent iron in the framework has motivated us for searching for trivalent chromium analogue, which would be the first example of Cr(III)-based luminescent metal formate

templated by protonated amine. It should be noted that although many luminescent MOFs are known, where luminescence arise from organic ligands, divalent metal transition ions or rare-earth ions,[3] Cr(III)-based luminescent MOFs are very scarce.[13,14] There are also very few examples of luminescent heterometal-organic frameworks.[3] We also hoped that substitution of Fe(III) by Cr(III) would help to understand relationship between chemical composition of the framework and structural as well as electric properties of this family of compounds. This effect has not been deeply studied since apart of the mentioned above DMNaFe, only three heterometallic or mixed-valence formates are known, that is, $[(CH_3)_2NH_2][Fe^{III}M^{II}(HCOO)_6]$ with M=Mn, Fe, Co, which crystallize in the niccolite-type structure.[15]

Experimental

Materials and instrumentation

HCOONa (99%, Fluka), $Cr(NO_3)_3 \bullet 9H_2O$ (99%, Aldrich), DMA•HCl (DMA•HCl = dimethylamine hydrochloride) (99%, Aldrich) and N,N-dimethylformamide (DMF) (99.8%, Aldrich) were commercially available and used without further purification. DSC was measured using Mettler Toledo DSC-1 calorimeter and nitrogen as a purging gas. Weight of DMNaCr sample was 19.2 mg. The heating and cooling rate was 5 K/min. The dielectric measurements were performed using a Novocontrol Alpha impedance analyzer (10^{-1}-10^{6} Hz). Due to small size of the crystals, pellet made of well-dried sample was measured instead. The pellet with thickness of 0.4 mm was located between two copper electrodes of the capacitor. The temperature was controlled by the Novo-Control Quattro system and a nitrogen gas cryostat. The measurements were taken every 1 deg over the temperature range from 120 to 270 K. Temperature stability of the samples was better than 0.1 K. Electron reflectance spectra were measured using a Cary 5E

spectrophotometer with the Praying Mantis diffuse reflectance accessory. For spectroscopic measurements at 300 K and 77 K Hamamatsu photonic multichannel analyzer PMA-12 equipped with BT-CCD linear image sensor and Nd:YAG laser as the excitation source were used. Temperature of 77 K were obtained using liquid nitrogen and a Dewar flask. To measure decay profiles, we used McPherson optical measurement system with Nd:YAG laser as the excitation source, Hamamatsu R928 photomultiplier as detectors and a digital oscilloscope RIGOL DS4052. For measurements at 10 K Jobin-Yvon measurement system along with helium close cycle cryostat was used. Decay profiles at 10 K were recorded with a Lecroy digital oscilloscope. Raman spectra were measured using a Renishaw InVia Raman spectrometer equipped with confocal DM 2500 Leica optical microscope and a thermoelectrically cooled CCD as a detector. The 488 nm line of an argon laser was used as excitation. Temperature-dependent IR spectra were measured for the samples in KBr pellets in the range of 3500-400 cm^{-1} and in Apiezon N suspension in the range of 500-50 cm^{-1} with the Biorad 575C FT-IR spectrometer using a helium-flow Oxford cryostat. The spectral resolution was 2 cm^{-1}.

Synthesis of the sample

To obtain DMNaCr, a mixture of $Cr(NO_3)_3 \bullet 9H_2O$ (4 mmol), HCOONa (12 mmol), DMA•HCl (4 mmol), DMF (35 mL), and H_2O (25 mL) was heated at 140 °C in a Teflon-lined microwave autoclave for 48 h. Small dark green crystals obtained after one week crystallization at room temperature were filtered from the mother liquid and washed by ethanol. The yield is about 55 % based on the starting chromium salt. A good match of its powder XRD pattern with the calculated one based on the single-crystal structure (see Figure S1) confirmed the phase purity of the bulk sample.

Crystallographic Structure Determination

Single-crystal x-ray diffraction data were collected at 302 and 115 K on a 4-circle diffractometer KM4CCD (Oxford Diffraction) using a graphite monochromated MoKα radiation (λ= 0.71073 Å). The low temperature was maintained by open-flow nitrogen gas system (Oxford Cryosystem). The CrysAlis software version 1.170.33.42 was used for data processing.[16] An empirical absorption correction was applied using spherical harmonics implemented in SCALE3 ABSPACK scaling algorithm. The structure was solved by direct methods and refined by the full-matrix least-squares method by means of SHELX-97 program package.[17] The results of the data collection and refinement along with the crystal description are presented in Table S1.

In addition, powder XRD pattern was obtained on an X'Pert PRO diffractometer equipped with PIXcel ultra-fast line detector, focusing mirror and Soller slits for CuKα_1 radiation (λ=1.54056 Å).

Results and discussion

Thermal Properties

The DSC measurements show no heat anomaly in the temperature range studied (125-350 K, Figure S2). This behavior is distinct from that found for isostructural DMNaFe, which showed presence of heat anomaly due to an order-disorder phase transition at 170.8 K upon heating and 167.0 K upon cooling.[12]

Structural Studies

The compound crystallizes in the trigonal structure, space group $R\bar{3}$. The same space group was reported recently for DMNaFe.[12] However, the both structures are slightly different since in

DMNaFe the Na and Fe atoms are located at 3a and 3b sites, respectively, whereas in DMNaCr the 3a sites are occupied by the Cr atoms and th3 3b sites by the Na atoms. The rigid framework built up of NaO_6 and CrO_6 octahedra, which are bridged by formate ions in the anti-anti mode configuration, accommodates DMA^+ cations in the large cavities (Figure 1 and S3). The Na-O distances (2.4201 Å, see Table 1) are very similar to those found in DMNaFe (2.4143 Å[12]) whereas the Cr-O distances (1.9806 Å) are slightly shorter than the Fe-O distances in DMNaFe (2.0121 Å). Similarly as in DMNaFe, the formate units in DMNaCr are strongly asymmetric, with the C-O bonds of 1.2321 and 1.2605 Å (Table 1). However, this asymmetry is smaller than in DMNaFe, for which the corresponding C-O bond lengths are 1.2171 and 1.2672 Å.[12] DMA^+ cation forms extensive hydrogen bonds to the metal formate framework. However, the hydrogen bonds are too weak to overcome thermally activated motions of DMA^+ and, as a result, these cations are dynamically disordered at room temperature (Figure 1). Table 2 shows the geometric parameters of the N-H···O hydrogen bonds between the DMA^+ cations and the anionic framework. The geometry of the hydrogen bonds in DMNaCr is very similar to that reported for DMNaFe,[12] that is, the N-H···O hydrogen bonds formed between DMA^+ and NaO_6 are stronger (the N···O distances are 2.877 and 3.065 Å) than the hydrogen bonds between DMA^+ and CrO_6 (the N···O distances are 3.099 and 3.537 Å). Furthermore, the N···O distances are very similar for DMNaCr and DMNaFe, suggesting very similar hydrogen bond strengths. It is worth noting, however, that some of the H···O distances are shorter in DMNaCr than in DMNaFe. For instance, the 2.017 and 2.358 Å distances in DMNaFe,[12] correspond to the 1.93 and 2.32 Å in DMNaCr. This result could indicate slightly stronger hydrogen bonds in DMNaCr than DMNaFe. However, X-ray diffraction is not very precise experimental method for location of hydrogen atoms in a structure and it is, therefore, better to take into account the N···O distances that are very similar for the both compounds. Moreover, IR data show nearly the same frequencies for the N-H

stretching vibrations of DMNaFe and DMNaCr (see the next paragraph) and this clearly confirms that the hydrogen bond strength is very similar in both compounds.

With temperature lowering, down to 115 K, the crystal structure remains stable and the interatomic distances of the framework change weakly (Table 1). The number of disordered DMA^+ orientations does not change so does the geometry of hydrogen bonding.

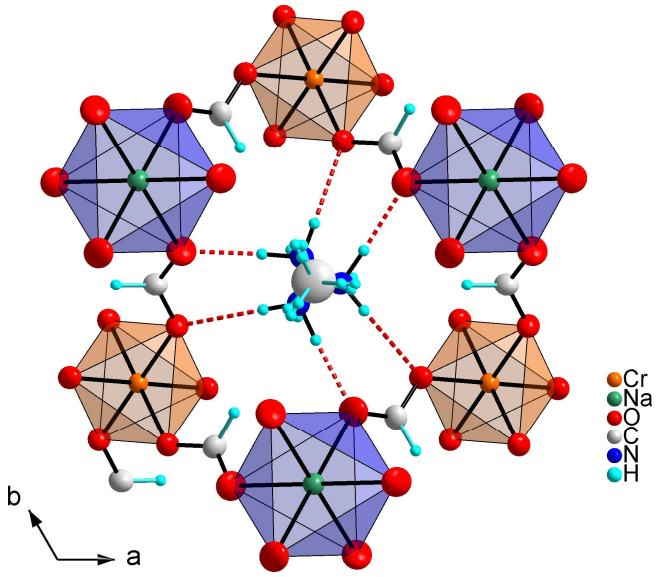

Figure 1. Distribution of disordered DMA^+ cations around trigonal 3 axis in the crystal cage at 302 K. Equivalent H-bonds are shown as dashed lines.

Table 1. Selected geometric parameters (Å) in DMNaCr.

	302 K	**115 K**
Na1-O1 × 6	2.4201(11)	2.4023(9)
Cr1-O2 × 6	1.9806(10)	1.9794(10)
C0-O1	1.2321(19)	1.2318(18)
C0-O2	1.2605(15)	1.2794(13)
C0-H0	1.0588	1.0648

N1-C1	1.308(5)	1.307(4)
N1-C2	1.432(5)	1.437(3)

Table 2. The geometries of the N-H···O bonds between the DMA^+ cations and the anionic framework at 302 and 115 K (distances, Å; angles, °).

D-H···A	d(D-H)	d(H···A)	d(D···A)	<(DHA)
303 K				
N(1)-H(1D)...O(1)#22	0.85	2.41	3.065(4)	134.1
N(1)-H(1D)...O(2)#23	0.85	2.32	3.099(4)	151.5
N(1)-H(1E)...O(1)#24	0.95	1.93	2.877(4)	170.2
N(1)-H(1E)...O(2)#20	0.95	2.83	3.537(4)	131.7
115 K				
N(1)-H(1D)...O(1)#22	0.86	2.40	3.036(4)	130.7
N(1)-H(1D)...O(1)#23	0.86	2.29	3.094(4)	154.2
N(1)-H(1E)...O(1)#24	0.99	1.91	2.884(4)	167.8
N(1)-H(1E)...O(2)#20	0.99	2.81	3.537(4)	131.1

Symmetry transformations used to generate equivalent atoms:

#20 x+1/3,y-1/3,z-1/3, #22 -x+y+1/3,-x+5/3,z-1/3, #23 -x+y-2/3,-x+2/3,z-1/3

#24 x-2/3,y-1/3,z-1/3

Dielectric Properties

Figure 2 shows the temperature dependence of dielectric permittivity for DMNaCr sample at several frequencies from the range of 10 Hz to 2 MHz. The real part of dielectric permittivity ε'(T) takes fairly modest value similar to that observed for DMNaFe.[12] The results show that the

broad maximum of ε'(T) is shifted towards higher temperature region with increasing frequencies. Such behavior implies the relaxor character of the investigated sample. At the same time, the imaginary part of dielectric permittivity ε"(T) exhibits a peak shifted towards higher temperatures with increasing frequency.

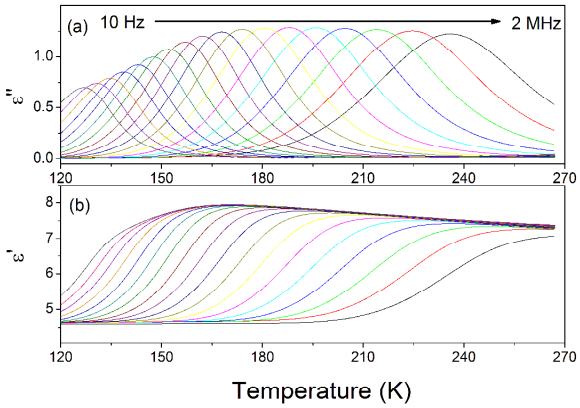

Figure 2. Variation of the real ε' and imaginary ε" part of the complex dielectric permittivity at frequency range from 10 Hz to 2 MHz in the 120-270 K temperature range. The data were collected during heating process. The arrow points the direction of the peak positions shift with increasing measuring frequency.

In order to identify the nature of relaxation process occurring in the material the temperature dependence of resonant frequency $\ln(f_r)$ vs T_m plot was considered (Figure 3). Nonlinear dependence of this relation confirms that the relaxation of such a highly disordered systems, like the one we were dealing with, does not follow the classical Arrhenius temperature behavior. In such materials the relaxation time on cooling tends to infinity at a nonzero temperature T_{VF}. The T_{VF} can be considered as the freezing temperature below which the system becomes nonergodic. In order to analyze the relaxation features at $T > T_{VF}$, the Vogel-Fulcher law may be used:

$$f_r = f_0 e^{\frac{E_a}{k(T-T_{VF})}} \quad (1)$$

where f_0 is the attempt frequency, E_a is an activation energy, k is the Boltzmann's constant and T_{VF} is the freezing temperature. E_a represents the activation energy for induced polarization of an isolated cluster. In the case of DMNaCr, an isolated cluster corresponds to DMA^+ cation interacting with $HCOO^-$ ion *via* hydrogen bond. These clusters may interact *via* dipole-induced dipole exchanges or elastically through local rhombohedral distortions implying that the clusters may freeze into an orientational glassy state. Analysis of the obtained results gave a preexponential factor f_0 of 2.5±0.5 x 10^{12} Hz, an activation energy of 0.28±0.02 eV, and static freezing temperature of 5.0±3.0 K. The curve fitting to the data is shown as the solid line in Figure 3. Good agreement of the experimental data with Vogel-Fulcher approximation, suggests the relaxor behavior of the DMNaCr, analogous to spin glass with local polarization fluctuations above a static freezing temperature.[18] It should be noted that the same 0.28 eV value of the activation energy for reorientational motions of DMA^+ was also found for DMNaFe,[12] implying that the polar DMA^+ ion is confined with the same strength by the DMNaCr and DMNaFe frameworks.

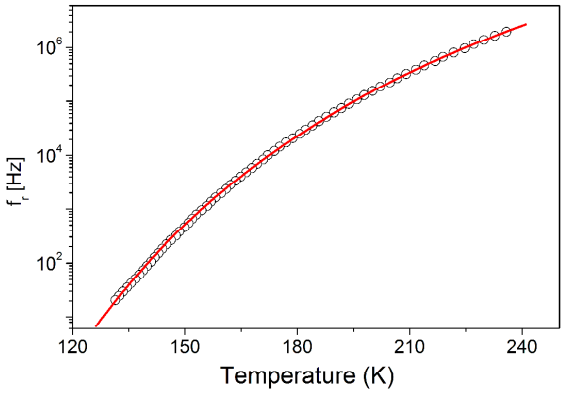

Figure 3. Frequency corresponding to the dielectric permittivity ε" maximum as a function of temperature.

In Figure 4 dielectric response of the studied material is presented. It is clear from the plot that imaginary part of dielectric permittivity exhibits single relaxation peak, shifted towards higher frequencies with increasing temperature. The observed dielectric response of the sample deviates from the classical Debye behavior. The sample exhibits the anomalous relaxation mechanism represented by low- and high-frequency power-law dependence of the imaginary part of dielectric permittivity on frequency, i.e.:

$$\varepsilon''(\omega) \propto (\omega/\omega_p)^m \quad \text{for} \quad \omega < \omega_p,$$
$$\varepsilon''(\omega) \propto (\omega/\omega_p)^{n-1} \quad \text{for} \quad \omega > \omega_p, \qquad (2)$$

where ω_p denotes the loss peak frequency and the power-law exponents fall in the range $0 < m, n < 1$. Such a relaxation pattern is specific for complex materials of locally random characteristics. The deviation of the dielectric data from the exponential response can be observed also on a complex plane representation (Figure 5). The loss peak is slightly asymmetric and it is narrower than a pure Debye peak.

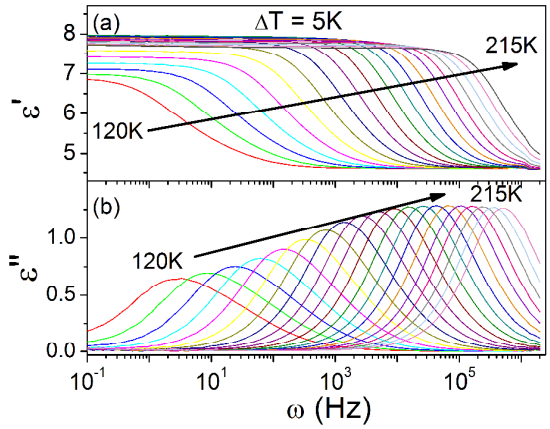

Figure 4. Frequency dependence of real ε' (a) and imaginary ε" (b) part of the complex dielectric permittivity.

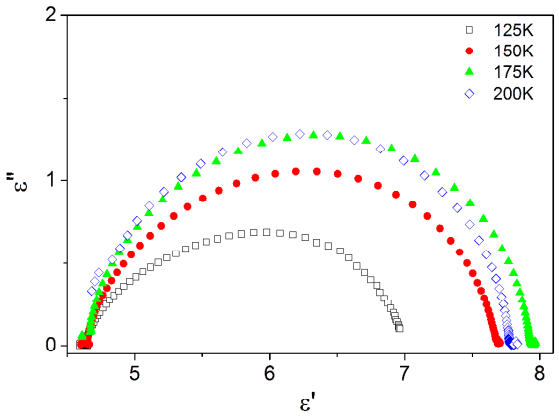

Figure 5. Complex permittivity diagram (Cole-Cole plot) at a few temperatures.

Vibrational Studies

The Raman and IR spectra of DMNaCr are presented in Figures 6, 7 and S4-S6, Supporting Information. The observed IR and Raman frequencies are listed in Table S2, Supporting Information, together with proposed assignments of modes to respective motions of atoms in the unit cell. The assignment of internal modes can easily be done by comparison of the present results with Raman and IR data obtained for isostructural DMNaFe.[12] This comparison shows that majority of DMNaCr modes differ from the respective modes of DMNaFe by less than 4 cm^{-1}. In particular, modes of the NH_2 groups are observed at almost the same frequencies for the both compounds. This behavior indicates very similar hydrogen bond strength in these compounds. This conclusion is further supported by observation of other DMA^+ modes at nearly the same frequencies for DMNaCr and DMNaFe. Contrary to DMA^+ modes, most of modes

attributed to $HCOO^-$ ions shift towards higher frequencies when iron is replaced by chromium (see Table S2). The largest shift (18 cm^{-1}) is observed for the ν_3 mode. This behavior can be attributed to changes in C-O bond lengths and O-C-O angles when Fe is replaced by Cr.

In the lattice modes region, Raman spectra of the both compounds are also quite similar. There are, however, significant shifts towards higher frequencies (up to 18 cm^{-1}) for the 178 and 60 cm^{-1} modes of DMNaCr attributed by us mainly to librational modes of the $HCOO^-$ ions (L(HCOO) modes, see Table S2). Even larger shifts towards higher frequencies are observed for the IR modes. For instance, the 350 cm^{-1} mode of DMNaFe corresponds to the 420 cm^{-1} mode of DMNaCr. Such pronounced shift can be attributed to smaller atomic mass of Cr (52.00) than Fe (55.85) and tighter binding of Cr(III) (the Cr-O distance is 1.9806 Å) than Fe(III) (the Fe-O distance is 2.0121 Å[12]).

Temperature-dependent spectra show narrowing of bands and slight shifts (see Figures, 6, 7 and S4-S6). As a result some additional bands, not resolved at room temperature, become clearly visible at low temperatures, especially below 140 K. For instance, the IR bands corresponding to the $\tau(CH_3)$ mode is overlapped by the broad band at 276 cm^{-1} but becomes well resolved below 140 K and is observed at 296 cm^{-1} at 5 K (see Figure S6 and Table S2). In general, the most significant narrowing is observed for the lattice modes and the internal modes of the NH_2 group. This behavior can be attributed to slowing down of reorientational motions of DMA^+ cations with decreasing temperature. Comparison of the DMNaCr and DMNaFe data shows, however, significant differences between these compounds. Firstly, the observed narrowing is much less pronounced for DMNaCr (see Figures 6, 7 and S4-S6). For instance, FWHM of the 1337 cm^{-1} band of DMNaCr decreases from 14.7 cm^{-1} at 294 K to 9.3 cm^{-1} at 80 K whereas the corresponding band of DMNaFe narrows from 15.2 to 7.2 cm^{-1} at 90 K and 5.7 cm^{-1} at 7 K. Secondly, some bands of DMNaCr exhibit narrowing but they split for DMNaFe. For instance,

the FWHM of the 342 cm^{-1} Raman band of DMNaCr decreases from 19.4 cm^{-1} at 294 K to 11.1 cm^{-1} at 80 K whereas the corresponding band of DMNaFe is very broad at room temperature, with FWHM of 47.2 cm^{-1}, and splits into three narrow bands at 333, 343 and 356 cm^{-1} at 80 K.[12] Thirdly, in case of DMNaFe the $\rho(NH_2)$ IR band was clearly split at 5 K into two components at 907 and 913 cm^{-1}, with FWHM values of 11.9 and 7.7 cm^{-1}, respectively (see Figure 6 (b) and Ref. 12). This behavior proves the presence of two crystallographically distinct DMA^+ cations in the low-temperature phase of DMNaFe. The IR spectrum of DMNaCr shows presence of only one broad band at 908 cm^{-1} with FWHM of 18.6 cm^{-1}. It is worth noting that the $\rho(NH_2)$ band is very sensitive to disorder of DMA^+ cations and its FWHM value was about 5 cm^{-1} for well ordered DMA^+ cations in the low-temperature phases of DMMn, DMNi and DMZn.[7,19] All these facts prove that contrary to DMNaFe, which undergoes a structural phase transition associated with ordering of DMA^+ cations and distortion of the metal formate framework, DMNaCr does not exhibit any structural phase transition down to 5 K.

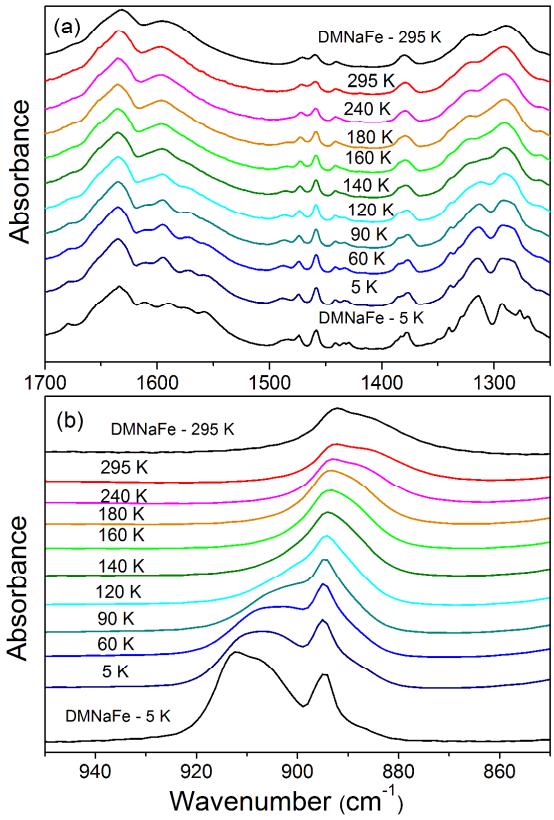

Figure 6. Detail of the IR spectra of DMNaCr results corresponding to the spectral ranges (a) 1250-1700 cm^{-1} and (b) 850-950. For the comparison sake, spectra of DMNaFe at 295 and 7 K are also shown.

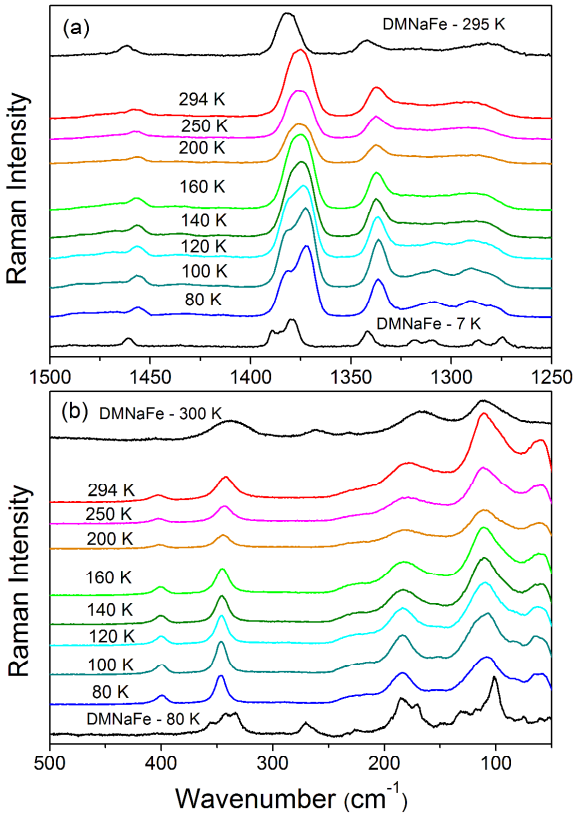

Figure 7. Detail of the Raman spectra of DMNaCr results corresponding to the spectral ranges (a) 1250-1500 cm^{-1} and (b) 50-500 cm^{-1}. For the comparison sake, spectra of DMNaFe at two temperatures are also shown.

Optical Studies

The room-temperature **e**mission band, observed at 787.6 nm, is very broad with FWHM value of 2452 cm^{-1} (see Figure 8). In addition to the broad band, small humps are observed at 687.6, 698.9, and 707.9 nm. The broad band is assigned to the $^4T_{2g} \rightarrow {}^4A_{2g}$ transition, and the small humps appear due to the $^2E_g \rightarrow {}^4A_{2g}$ spin forbidden transitions. It should be noted that the energy of the $^2E_g \rightarrow {}^4A_{2g}$ transitions is similar to that found in the inorganic compounds.[20] This

behavior is very different to that found for chromium(III) terephthalate [$Cr_3O(C_8H_4O_4)_3F(H_2O)_2$] (MIL-101), for which the $^2E_g \rightarrow {}^4A_{2g}$ emission band was observed near lower energy, i.e. 790 nm, due to the electronic interaction in the metal-organic framework of this compound, which resulted in the partial delocalization of an excited electron in Cr(III).[14]

The $^4T_{2g}/^2E_g$ intensity ratio decreases from 48 % at room temperature to 6 % at 77 K, that is, the peaks associated with the $^2E_g \rightarrow {}^4A_{2g}$ transition dominate the low temperature spectrum. Furthermore, maximum of the broad band shifts to 818.4 nm and new narrow bands appear at longer wavelength (see inset in Figure 8). When temperature decreases to 10 K, the spectrum shows presence of many narrow bands. Energies of these bands are listed in Table 3 together with tentative assignment. In the spectrum recorded at 10 K, the R_1 line at 14495.3 cm^{-1} (689.88 nm) becomes the most intense. Separation between the R_1 and R_2 lines is 48.8 cm^{-1}, indicating relatively strong influence of the crystal field on energy levels of the chromium ions in DMNaCr. The line at 14331 cm^{-1} decreases strongly with decreasing sample temperature. This behavior proves its vibronic character. Contrary to this line, the three lines observed at 14118.4, 13724.3, and 13233.8 cm^{-1} do not change their intensity at low temperature. Since the crystal is heavily doped with chromium, we assign them to the chromium pair lines, whereas other less intense lines are due to vibronic transitions associated with both R and pair lines (see Table S3). We have found no evidence for chromium ions located at different sites; broad emission bands are symmetric with well-defined one maximum both at 300 and 77 K. Moreover, the narrow lines can be assigned to single Cr(III) site electric-dipole character transitions and associated with them vibronic lines.

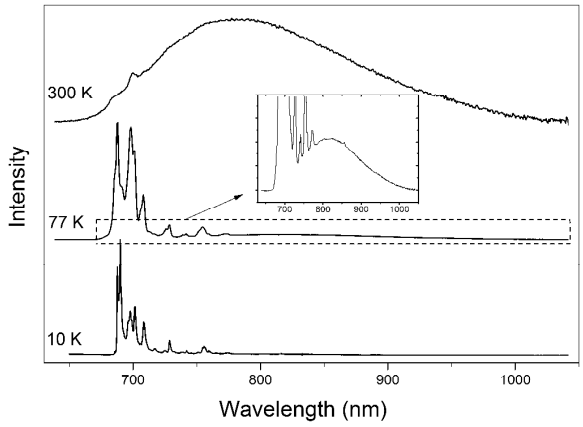

Figure 8. Emission spectra of DMNaCr recorded under 532 nm excitation. Inset shows magnified $^4T_{2g} \rightarrow A_{2g}$ emission recorded at 77 K.

Absorption spectrum is characteristic for Cr(III) ions located at intermediate ligand field (see Figure 9). Three broad bands centered at 17600, 24220, and 42000 cm^{-1} were assigned according to O_h notation to the transitions from the ground $^4A_{2g}$ level to the $^4T_{2g}$, $^4T_{1g}$(F), and $^4T_{1g}$(P) levels, respectively. The small hump visible at 14544 cm^{-1} can be assigned to the $^2E_g \rightarrow {}^4A_{2g}$ spin forbidden transition. The bands are broadened and the two later ones are split into two components due to lower than O_h symmetry, which removes the degeneracy of the energy levels. The splitting is relatively large (see Table 3). For example, in the spinel structure of Cr(III) doped $ZnAl_2O_4$, the splitting of the $^4T_{1g}$ band is 1860 cm^{-1} whereas in the natural and synthetic $MgAl_2O_4$, the splitting is 1700 and 2500 cm^{-1}, respectively.[21] On the other hand the large width of the $^4T_{1g}$ band could be associated with multiple chromium sites; however there is no evidence of different chromium sites neither from crystallographic data nor from emission spectra.

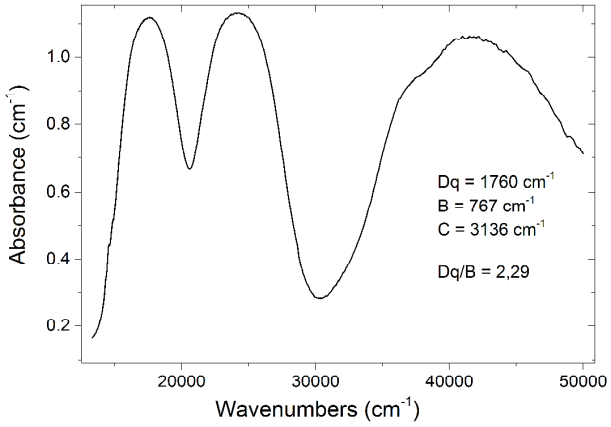

Figure 9. The 300 K diffuse reflectance spectrum of DMNaCr.

Table 3. Energy levels of Cr^{III} ions in DMNaCr.

Label	Energy (cm^{-1})
^2E_g	14544
	14495
$^4T_{2g}$	16364
	18756
$^4T_{1g}(F)$	22184
	25098
$^4T_{1g}(P)$	36641
	43744

Absorption spectrum served for calculation of the crystal field parameter Dq and Racah parameters B and C. Value of the B parameter was found computing when the determinant (where: T_F is energy of the $^4T_1(F)$ band) defined below is equal 0.

$$\begin{vmatrix} 10Dq + 12B - T_F & 6B \\ 6B & 20Dq + 3B - T_F \end{vmatrix} \quad (3)$$

C parameter was calculated from:

$$C = E_g + 1.8\frac{\frac{B^2}{Dq} - 7.9B}{3.05} \quad (4)$$

The calculated values are Dq = 1760 cm^{-1}, B = 767 cm^{-1}, C = 3136 cm^{-1}. Thus the ratio Dq/B = 2.29 and C/B = 4.1. On the Tanabe Sugano diagram the ^2E_g and $^4T_{2g}$ levels overlap for Dq/B = 2.3. This point separates so called weak (Dq/B < 2.3) and strong (Dq/B > 2.3) ligand field. For the former the $^4T_{2g}$ level is the lowest one and only from this level broad emission is observed. In our sample emission character depends on temperature at which measurements are performed; at room temperature broad emission is observed whereas at 77 K and lower temperature narrow spin-forbidden lines are observed (see Figure 8). Such situation occurs in the so called intermediate ligand field, where minima of the both levels, i.e. the $^4T_{2g}$ and ^2E_g ones, lie close each other and the latter is located slightly below the first one. At room temperature the doublet level serves as an energy reservoir for the quartet one, and broad allowed by the selection rules emission is observed. At low temperatures, when vibronic sub-levels are empty, energy from the quartet level is drained quickly to the doublet level and mainly narrow spin-forbidden transition is observed. However the broad emission, although seven times smaller than at room temperature, is still observed. This is well depicted in observation of the emission decay profiles shown in Figure 10. The decay profile from the R line is single exponential at 10 K with decay constant equal 430 μs. The emission decay time of the R line is substantially shorter (only 30 μs)

at 77 K. The shortening of the R line emission decay time is due to two factors. First, rate of nonradiative transitions caused by donor-donor energy transfer (the sample is heavily doped with chromium ions) increases. Second, the ^2E_g level transfers the energy to the $^4T_{2g}$ level. This transfer is proportional to the ΔE energy separation between the ^2E_g and $^4T_{2g}$ levels and the observed decay time τ is proportional to the following equation:

$$\frac{1}{\tau} \propto \frac{\frac{1}{\tau_4} + \frac{1}{\tau_2}}{1 + \exp[-\Delta E/k_B T]} \quad (5)$$

where τ_4 and τ_2 are decay time of the quartet and doublet level, respectively, k_B is Boltzmann constant and T is temperature. $1/\tau$ approaches $1/\tau_2$ when $T \rightarrow 0$, and $(1/\tau_2 + 1/\tau_4)/2$ when $T \rightarrow \infty$. At room temperature only emission from the $^4T_{2g}$ level is observed and its decay time is equal 17 μs. Decay profile is non-exponential due to strong donor-donor energy transfer caused by the high level Cr(III) doping.

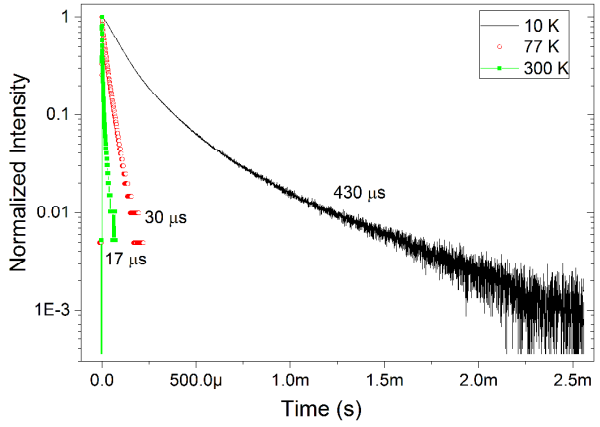

Figure 10. Decay profiles of DMNaCr luminescence recorded at 10 K monitored at 698.9 nm, at 77 K monitored at 687.5 nm, and at 300 K monitored at 780 nm measured under 532 nm excitation (color online).

Origin of different structural stability of DMNaCr and DMNaFe

Our studies show that DMNaCr is isostructural to the known DMNaFe. In the both compounds the DMA^+ cations are disordered and connected with the metal formate framework *via* hydrogen bonds of very similar strength. Dielectric, Raman and IR data show that upon cooling, the reorientational motions of DMA^+ cations slow down. When temperature decreases to about 170 K, an order-disorder phase transition occurs in DMNaFe.[12] The ordering of DMA^+ cations is associated with triclinic distortion of the framework.[12] Contrary to DMNaFe, freezing of the molecular rotation of DMA^+ in DMNaCr does not result in any structural phase transition, i.e., DMA^+ cations statistically occupy three equivalent positions around the threefold axis in the low-temperature phase. In other words, the dynamical disorder observed at room temperature evolves upon cooling into a statistical one and the anionic framework is not distorted.

The question that rises is what is the reason for lack of a structural phase transition in DMNaCr. To understand this behavior, it is worth noting that the driving force the phase transitions in DMNaFe, $[(CH_3)_2NH_2][Fe^{III}Fe^{II}(HCOO)_6]$ and $[(CH_3)_2NH_2][M(HCOO)_3]$, where M=Mg, Zn, Mn, Ni, Co, Fe, was assumed to be mainly the cooperative freezing of the molecular rotation of the DMA^+ cations, rather than distortion of the metal formate framework.[7,10,12,15] Indeed, the host frameworks constructed from $HCOO^-$ ligands are relatively stiff but studies of $[(CH_3)_2NH_2][Cd(N_3)_3]$ with more flexible azido framework showed that for this compound the driving force for the phase transition is mainly the deformation of the $[Cd(N_3)_3]^-$ framework accompanied by simultaneous change in the rotational motion of DMA^+ ion.[22] Thus depending on the flexibility of the framework, the mechanism initially responsible for a phase transition in the alkylammonium metal formates may be either ordering of alkylamonium cations or deformation of the framework. But in both cases both ordering of cations and distortion of the

fremework are observed simultaneously. It should be noticed that Sanchez-Andujar *et al.* also suggested that properties of the framework may play significant role in the phase transition, that is, the phase transition may occur only when the metal formate framework is flexible enough to allow tilting of the MO_6 octahedra.[23] Our present data give strong support to this idea. Namely, they clearly show that replacement of Fe(III) by Cr(III) in the framework results in disappearance of the phase transition. This behavior cannot be attributed to different confinement of the DMA^+ in DMNaCr and DMNaFe since x-ray diffraction and dielectric data show that the DMA^+ ions are confined with approximately the same strength in the both frameworks. It cannot also be attributed to different distortion of the MO_6 octahedra since this distortion is small and similar in the both frameworks at room temperature. This can be quantified by calculating the distortion parameter Σ:

$$\Sigma = \sum_{i=1}^{12} \left(\left| \varphi_i - 90 \right| \right) \quad (6)$$

where φ_i denote 12 *cis* O-M-O angles in the coordination sphere.[24] The distortion parameters Σ are 10.54° and 6.96° for FeO_6 and NaO_6 in DMNaFe, and 9.60° and 9.96° for CrO_6 and NaO_6 in DMNaCr. We suppose, therefore, that different behavior of DMNaCr and DMNaFe can be attributed to different flexibilities of the frameworks, that is, DMNaCr has a less flexible framework than DMNaFe due to a smaller ionic radius of the chromium ions. Due to less flexible framework, the strength of hydrogen bonds in DMNaCr is not large enough to force distortion of the framework at low temperatures. Indeed, the distortion parameters Σ for DMNaCr at 115 K are still small, i.e., 11.88° and 6.12° for CrO_6 and NaO_6. Similar hydrogen bond strength is, however, sufficient to lead to distortion of more flexible framework in DMNaFe. As a result, the

distortion parameters Σ calculated for the DMNaFe stucture at 110 K are large, i.e., 67.21° and 62.07° for FeO_6 and NaO_6, respectively. It is worth noting that studies of $[(CH_3)_2NH_2][Cd(N_3)_3]$ and $[(CH_3)_2NH_2][Mn(N_3)_3]$ isostructural compounds also showed very different behavior of these compounds, indicating that change of the metal ion can modulate the flexibility of the perovskite-like framework to tune its structural and related physical properties.[22,25] Our results show that also in the less flexible frameworks constructed from two types of metal ions and formate ligands, change of the metal ion in the framework may significantly tune its flexibility and structural stability.

Conclusions

We have synthesized novel heterometallic formate templated with DMA^+ cations, crystallizing in the perovskite architecture with dynamically disordered DMA^+ cations. Upon cooling, the reorientational motions of DMA^+ cations slow down and this process gives rise to relaxor-like dielectric response. In spite of freezing of the molecular rotation of DMA^+ cation, no evidence for structural phase transition is found for DMNaCr, although clear distortion of the structure was observed for isostructural DMNaFe. Thus subtle change of the coordination parameters when Cr(III) is substituted for Fe(III) leads to very pronounced change in the structural stability of the framework. This behavior proves that properties of the metal framework play important role in the stabilization of the structure. In particular, if the hydrogen bond strength between the organic cation and anionic framework is too weak and/or the framework is too rigid, the dynamical disorder will evolve into static one and no phase transition will be observed. No low-temperature phase transition will be observed also if the hydrogen bond strength is too large and the anionic framework too flexible: in such cases the organic cations will be ordered already at

room temperature. Thus structural stability of these compounds is governed by a complex interplay between different types of bonding interactions, such as hydrogen bonding and ionic interactions, and a structural phase transition may occur only for those MOFs, which are characterized by some specific balance between strength of the hydrogen bonds and flexibility of the framework. This explains why most of the synthesized metal formates templated by organic cations do not exhibit any structural phase transitions.

We have also presented detailed studies of optical properties. They show that emission and absorption properties of DMNaCr are characteristic for Cr(III) ions located at intermediate ligand field. The emission is strong at low temperatures, in spite of large concentration of Cr(III) ions and thus concentration quenching of emission. It would be, therefore, of interest to synthesize Cr(III)-doped DMNaFe or yet unknown DMNaM, where M=Al, Sc or In since such compounds with small concentration of Cr(III) may exhibit better luminescent properties.

Acknowledgements

This research was supported by the National Center for Science (NCN) in Poland under project No. DEC-2011/03/B/ST5/01019.

Notes

[a]Institute of Low Temperature and Structure Research, Polish Academy of Sciences, Box 1410, 50-950 Wrocław 2, Poland; m.maczka@int.pan.wroc.pl; phone: +48-713954161; fax: +48-713441029

[b]Institute of Physics, Wrocław University of Technology, Wybrzeże Wyspiańskiego 27, 50-370

Wrocław, Poland

Electronic Supplementary Information (ESI) available: X-ray crystallographic information files (CIF) for crystal structures of DMNaCr at 302 and 115 K. Figures S1-S6: Powder X-ray diffraction, DSC traces, view of the crystal structures, IR and Raman spectra. Tables S1-S3: X-ray data collection and refinement parameters, Raman and IR frequencies, and energies of emission bands.

References

1 W. Zhang and R. G. Xiong, *Chem. Rev*., 2012, **112***,* 1163.

2 R. J. Kuppler, D. J. Timmons, Q. R. Fang, J. R. Li, T. A. Makal, M. D. Young, D. Yuan, D. Zhao, W. Zhuang, H. C. Zhou, *Coord. Chem. Rev.,* 2009, **253,** 3042.

3 Y. Cui, Y. Yue, G. Qian, B. Chen, *Chem. Rev.,* 2012, **112,** 1126.

4 L. E. Kreno, K. Leong, O. K. Farha, M. Allendorf, R. P. V. Duyne, J. T. Hupp, *Chem. Rev.,* 2012, **112,** 1105.

5 R. Shang, S. Chen, Z. M. Wang, S. Gao, in *Metal-Organic Framework Materials*. Edited by R. L. MacGillivray and C. M. Lukehart., John Wiley & Sons Ltd., 2014, pp. 221-238.

6 *(a)* P. Jain, N. S. Dalal, B. H. Toby, H. W. Kroto, A. K. Cheetham, *J. Am. Chem. Soc.* 2008, **130,** 10450; *(b)* D. W. Fu, W. Zhang, H. L. Cai, Y. Zhang, J. Z. Ge, R. G. Xiong, S. D. Huang and T. Nakamura, *Angew. Chem. Int. Ed*., 2011**, 50***,* 11947.

7 M. Mączka, A. Gągor, B. Macalik, A. Pikul, M. Ptak, J. Hanuza, *Inorg. Chem.* 2014, **53,** 457.

8 *(a)* M. Mączka, A. Pietraszko, B. Macalik and K. Hermanowicz, *Inorg. Chem*., 2014, **53**, 787; *(b)* R. Shang, G. C. Xu, Z. M. Wang, S. Gao, *Chem. Eur. J*. 2014, **20,** 1146.

9 A. Rossin, M. R. Chierotti, G. Giambiastiani, R. Gobetto and M. Peruzzini, *Cryst. Eng. Comm.,* 2012**, 14***,* 4454.

10 *(a)* P. Jain, V. Ramachandran, R. J. Clark, H. D. Zhou, B. H. Toby, N. S. Dalal, H. W. Kroto and A. K. Cheetham, *J. Am. Chem. Soc.,* 2009, **131***,* 13625; *(b)* G. C. Xu, W. Zhang, X. M. Ma, Y. H. Hen, L. Zhang, H. L. Cai, Z. M. Wang, R. G. Xiong and S. Gao, *J. Am. Chem. Soc.,* 2011**, 133***,* 14948; *(c)* W. Wang, L.-Q. Yan, J.-Z. Cong, Y.-L. Zhao, F. Wang, S.-P. Shen, T. Zhou, D. Zhang, S.-G. Wang, X.-F. Han and Y. Sun, *Sci. Rep*., 2013**, 3**, 2024.

11 A. Rossin, G. Giambiastiani, M. Peruzzini, R. Sessoli, *Inorg. Chem.* 2012, **51,** 6162.

12 M. Mączka, A. Pietraszko, L. Macalik, A. Sieradzki, J. Trzmiel, A. Pikul, *Dalton Trans.* 2014, ***43,*** 17075.

13 K. A. Kovalenko, D. N. Dybtsev, S. F. Lebedkin, V. P. Fedin, *Russ Chem. Bull. Int. Ed.* 2010, **59,** 741.

14 Y. Y. Liu, P. Yang, G. X. Du, B. Ding, X. G. Wang, *Synth. React. Inorg. Metal-Organic Nano-Metal Chem.* 2014, **44,** 22.

15 *(a)* K. S. Hagen, S. G. Naik, B. H. Huynh, A. Masello, G. Christou, *J. Am. Chem. Soc.* 2009, **131,** 7516; *(b)* L. Canadillas-Delgado, O. Fabelo, J. A. Rodriguez-Velamazan, M.-H. Lemee-Cailleau, S. A. Mason, E. Pardo, F. Lloret, J.-P. Zhao, X.-H. Bu, V. Simonet, C. V. Colin, J. Rodriguez-Carvajal, *J. Am. Chem. Soc*. 2012, **134,** 19772; *(c)* J.-P. Zhao, B.-W. Hu, F. Lloret, J. Tao, Q. Yang, X.-F. Zhang, X.-H. Bu, *Inorg. Chem*. 2010, **49,** 10390.

16 Agilent Technology Poland, CrysAlis RED, Data Reduction Program, Issue 171.33.42.

17 G. M. Sheldrick, *Acta Cryst. A* 2008, **64,** 112.

18 D. Viehland, S. J. Jang, E. Cross, M. Wuttig, *J. Appl. Phys*. 1990, **68,** 2916.

19 M. Mączka, M. Ptak, L. Macalik, *Vib. Spectrosc.* 2014, **71,** 98.

20 *(a)* J. Hanuza, M. Mączka, K. Hermanowicz, M. Andruszkiewicz, A. Pietraszko, W. Stręk, P. Dereń, *J. Sol. State Chem.* 1993, **105,** 49; *(b)* K. Hermanowicz, M. Mączka, P. J. Dereń, J. Hanuza, W. Stręk, H. Drulis, *J. Liminesc*. 2000, **92,** 151.

21 *(a)* W. Mikenda, A. Preisinger, *J. Luminesc*. 1981, **26,** 53; *(b)* P. J. Dereń, M. Malinowski, W. Stręk, *J. Luminesc*. 1996, **68,** 91.

22 Z. Y. Du, T. T. Xu, B. Huang, Y. J. Su, W. Xue, C. T. He, W. X. Zhang, X. M. Chen, *Angew. Chem. Int. Ed*. 2014, **126,** published on-line: DOI: 10.1002/anie.201408491.

23 M. Sánchez-Andújar, L. C. Gómez-Aguirre, P. Pato-Dolán, S. Yáñez-Vilar, R. Artiaga, A. L. Llamaz-Saiz, R. S. Manna, F. Schnelle, M. Lang, F. Ritter, A. A. Haghighirad and M. A. Señarís-Rodríguez, *Cryst. Eng. Comm*., 2014, **16,** 3558.

24 P. Guionneau, M. Marchivie, G. Bravic, J.-F. Letard, D. Chasseau, Topp. Curr. Chem. 2004, 234, 97.

25 X. H. Zhao, X. C. Huang, S. L. Zhang, D. Shao, H. Y. Wei, X. Y. Wang, *J. Am. Chem. Soc*. 2013, **135,** 16006.